



Using gate-modulated Raman scattering and electron-phonon interactions to probe single-layer graphene: A different approach to assign phonon combination modes

D. L. Mafra,^{1,2} J. Kong,² K. Sato,³ R. Saito,³ M. S. Dresselhaus,^{2,4} and P. T. Araujo^{2,*}

¹*Departamento de Física, Universidade Federal de Minas Gerais, 30123-970 Belo Horizonte, Brazil*

²*Department of Electrical Engineering and Computer Science, Massachusetts Institute of Technology, Cambridge, Massachusetts 02139, USA*

³*Department of Physics, Tohoku University, Sendai 980-8578, Japan*

⁴*Department of Physics, Massachusetts Institute of Technology, Cambridge, Massachusetts 02139, USA*

(Received 18 October 2012; published 30 November 2012; corrected 4 December 2012)

Gate-modulated and laser-dependent Raman spectroscopy have been widely used to study $q = 0$ zone center phonon modes, their self-energy, and their coupling to electrons in graphene systems. In this work we use gate-modulated Raman of $q \neq 0$ phonons as a technique to understand the nature of five second-order Raman combination modes observed in the frequency range of 1700–2300 cm^{-1} of single-layer graphene (SLG). Anomalous phonon self-energy renormalization phenomena are observed in all five combination modes within this intermediate frequency region, which can clearly be distinguished from one another. By combining the anomalous phonon renormalization effect with the double resonance Raman theory, which includes both phonon dispersion relations and angular dependence of the electron-phonon scattering matrix elements, and by comparing it to the experimentally obtained phonon dispersion, measured by using different laser excitation energies, we can assign each Raman peak to the proper phonon combination mode. This approach should also shed light on the understanding of more complex structures such as few-layer graphene (FLG) and its stacking orders as well as other two-dimensional (2D)-like materials.

DOI: [10.1103/PhysRevB.86.195434](https://doi.org/10.1103/PhysRevB.86.195434)

PACS number(s): 73.20.Hb, 73.22.-f, 78.30.Na, 78.67.Ch

I. INTRODUCTION

Raman spectroscopy is a powerful tool for the characterization of electrons and phonons, especially in carbon materials.^{1–5} In particular, gate-modulated and laser excitation energy (E_L) dependent Raman spectroscopy have been both widely used to distinguish the numbers of layers of a graphene flake,⁶ to distinguish the stacking order in flakes,^{7–11} and to study the phonon self-energy as well as electron-phonon interactions.^{12–18} In defect-free monolayer graphene, the G ($\sim 1582 \text{ cm}^{-1}$), G^* ($\sim 2450 \text{ cm}^{-1}$), and G' (or $2D$, $\sim 2700 \text{ cm}^{-1}$) features are the most prominent features in the Raman spectrum, and attention has been directed to those three modes regarding electrons, phonons, and their mutual interactions. While the G -band feature is a first-order process, the G^* and G' bands are second-order processes.^{19,20} The G -band [twofold feature involving the in-plane transverse optic mode (iTO) and the longitudinal optic mode (LO)] is a zone-center mode with a phonon wave vector $q = 0$. In contrast, the G^* ($iTO + LA$ $q \approx 2k$ and $2iTO$ $q \approx 0$) and the G' ($2iTO$ $q \approx 2k$) mode, where k is the electron wave vector, and q and k are measured from the \mathbf{K} point of the Brillouin zone (BZ), come from a double resonance Raman (DRR) process.^{19,21–23} The DRR process can be either an intravalley (AV) process, in which the photoexcited electron is scattered by a phonon to another point of the conduction band near the same Dirac point, or the electron is scattered by an intervalley (EV) process from the \mathbf{K} point to an inequivalent \mathbf{K}' point of the BZ, where both \mathbf{K} and \mathbf{K}' are at the edge of the BZ. The phonons involved in the AV process are around the Γ point or the center of the BZ, while the phonons involved in the EV process are around the \mathbf{K} point.

Recently, attention has also been given to studying some weak Raman features in the frequency range $1650 < \omega < 2300 \text{ cm}^{-1}$, which are associated with Raman combination

and overtone modes.^{7–10} Indeed, it has been shown that studies of the combination and overtone modes on few-layer graphene (FLG) can give us information about both the number of graphene layers in FLG and their stacking order.^{7,8,10} However, these works disagree with each other regarding the number of phonon peaks and the phonon assignments attributed to each peak.^{7–10} Since there are many possible combination modes in this frequency region and since the DRR mode frequencies are dispersive as a function of E_L ,²³ it has not been easy to determine the number of peaks and their individual dispersions. Additionally, it is now recognized that there are two $q \neq 0$ DRR conditions for the phonon wave vector: $q \approx 2k$ and $q \approx 0$ (measured from the \mathbf{K} point) which give different Raman peaks, some with and others without dispersive behaviors.^{24–26} Moreover, the phonon self-energy and the electron-phonon (el-ph) coupling associated with these combination and overtone modes have not yet been explored.

Concerning single-layer graphene (SLG), the first study of the combination modes in this frequency region between 1690 and 2150 cm^{-1} was reported by Cong *et al.*,⁷ where they show only three peaks (which are denoted in the present paper by peaks 1, 3, and 4, from the lowest to the highest frequency). They proposed their assignments to be combinations of the $q \neq 0$ phonon branches $LO + iTA$, $iTO + LA$, and $LO + LA$, from the lowest to the highest frequency, around the Γ point of the BZ, that is, all their peaks come from AV DRR processes. Rao *et al.*⁸ showed that there are two more peaks in this region, one around 1880 cm^{-1} (peak 2 in the present paper) and the other one around 2220 cm^{-1} (our peak 5). The 1880 cm^{-1} (2220 cm^{-1}) peak was tentatively assigned by them⁸ to the $q \neq 0$ $oTO + LO$ ($iTO + iTA$) phonon branch, both being an EV DRR process, that is, around the \mathbf{K} point of the BZ. However, by performing only E_L -dependent Raman experiments, it is not easy to properly assign the combination modes when these combination modes are close together in

frequency, even if we use the experimental information given by the phonon dispersion rate $\partial\omega/\partial E_L$ obtained from double resonance theory.^{22,23}

In this work we use additional information obtained from the phonon self-energies and angle-dependent el-ph matrix elements to properly assign phonon modes. Here it is shown that the \mathbf{k} -dependent electron-phonon interaction as investigated by studying the Raman spectra, as a function of both Fermi energy E_F by variation of both the gate voltage V_g and laser energy E_L , is important to give accurate/reliable information about the combination mode assignments and identification. Besides this, we show that gate-modulated Raman spectroscopy of $q = 0$ and $q \neq 0$ phonons provides a powerful approach to understand the nature and to assign phonon modes as well as their overtones and mutual mode combinations. We apply this approach to solve the uncertainty behind the phonon assignments of the Raman features between 1700 and 2300 cm^{-1} . The well known E_L -dependent experiment tells us which phonon branches could be involved in the processes, giving also their respective dispersion slopes which depend on graphene phonon velocities. First, we confirm the number of Raman peaks that are observed experimentally in this frequency range and we check which phonon mode assignment could be correct for each Raman peak by making a direct comparison between the experimental data and the theoretical phonon dispersion calculations.²⁷ Furthermore, for the Raman peaks that come from an EV DRR process, a discussion about the scattering directions, in terms of the high-symmetry directions $\mathbf{K}\Gamma$ and $\mathbf{K}M$, and of the various processes is important because the el-ph scattering matrix elements have a large k dependence (e.g., trigonal warping). The knowledge of the el-ph scattering matrix elements gives us more precise information on the \mathbf{q} phonon wave vector, vectorial dependence that is relevant for the DRR process.

Finally, we explore the phonon self-energy corrections for these $q \neq 0$ modes in SLG by varying the E_F of the system by an applied gate voltage (V_g). For all five observed Raman peaks in this frequency range, we can see a softening of the phonon frequency ω_q and a broadening of the phonon decay width γ_q as a function of E_F . These behaviors give us important and accurate information on the relevant Raman scattering processes, that is, whether a given Raman feature involves zone-center $q = 0$ phonons or if it is rather a DRR process involving $q \neq 0$ wave vector phonons.¹⁹ We show that by combining the DRR theory with these anomalous phonon renormalization effects we obtain a reliable and efficient technique of Raman spectroscopy for the assignment of combination phonon modes and overtones in monolayer graphene.

II. EXPERIMENTAL DETAILS

The Raman measurements were done in the back scattering configuration using a 2.10 and 2.16 eV (590 and 575 nm, respectively) dye laser, a 2.33 eV (532 nm) Nd:YAG laser, and a 2.54 eV (488 nm) argon laser, with a 100 \times objective. In all the cases, the laser power was kept around 1.5 mW to avoid heating effects. Our measurements were done on exfoliated graphene samples produced by the micromechanical cleavage

of graphite on a Si substrate covered with 300 nm of SiO_2 .^{6,28} The sample device was fabricated by lift-off patterning of thermally evaporated Cr/Au (5 nm/80 nm, respectively). Back gate measurements were done near room temperature with voltages in the range from -70 to 70 V. This corresponds to a Fermi energy E_F range from ~ -400 to ~ 400 meV by taking into account that E_F is related to V_g by $E_F = \hbar|v_F|\sqrt{\pi C_G(V_g - V_0)}/e$, where $v_F = 1.0 \times 10^6$ m/s is the Fermi velocity, $C_G = 1.15 \times 10^{-8}$ F/cm² is the geometric capacitance of the system, and V_0 is the gate voltage corresponding to the charge neutrality point, which is monitored by the V_g dependence of the G band frequency.

III. RESULTS AND DISCUSSION

A. E_L -dependent analysis

Figure 1(a) shows the combination modes in the spectral region from 1700 to 2300 cm^{-1} for four different laser lines: 488, 532, 575, and 590 nm. Each spectrum was fitted with five Lorentzians, in agreement with the number of peaks proposed by Rao *et al.*⁸ The experimental frequency dispersion of the five peaks taken from the fitting procedure applied to the Raman features in Fig. 1(a) were plotted together with the theoretical phonon dispersions of SLG adapted from the Popov and Lambin calculations that were performed within the tight-binding formulation, where the electronic trigonal warping effect of the graphene π bands was taken into account²⁷ [see Figs. 1(b) and 1(c)]. The symbols correspond to the frequencies of peaks 1 to 5 for each E_L along the high-symmetry line $\Gamma\mathbf{K}M$. Squares, circles, triangles, diamonds, and stars denote peaks 1 to 5, respectively. The full lines are the theoretical phonon branches²⁷ for the combination modes LO + iTA (black), iTO + LA (red), LO + LA (blue), oTO + iTO (purple), oTO + LO (gray), and iTO + iTA (green). The peak numbers given in Fig. 1(a) are written below the corresponding phonon branch assigned to each combination mode. When the peaks can be fitted to a phonon dispersion, we can assign the peak to a corresponding combination mode (Appendix A provides a detailed description of how we obtain the phonon momentum from an E_L -dependent experiment).

In Fig. 1(c) the experimental data were plotted considering the phonon assignments reported in the literature by Cong *et al.*⁷ and by Rao *et al.*⁸ Peaks 1, 3, and 4 coming from an AV DRR process and peaks 2 and 5 coming from an EV DRR process. Figure 1(c) shows that the assignments proposed in the literature^{7,8} for peak 1 as LO + iTA around the Γ point and for peak 5 as iTO + iTA around the \mathbf{K} point are in good agreement with the theoretical curve as regards both the frequency values and dispersion slopes. On the other hand, one can clearly see that peak 2 does not match well the proposed⁸ assignment of the oTO + LO combination mode around the \mathbf{K} point, and peak 3 is not in good agreement with the combination phonon branch iTO + LA around the Γ point. Due to the small energy difference between peaks 3 and 4 (around 30 cm^{-1}) and the similar dispersion values (see Table I), there is a clear ambiguity in the experimental assignment when made by using only laser-dependent measurements, as is now in common usage.

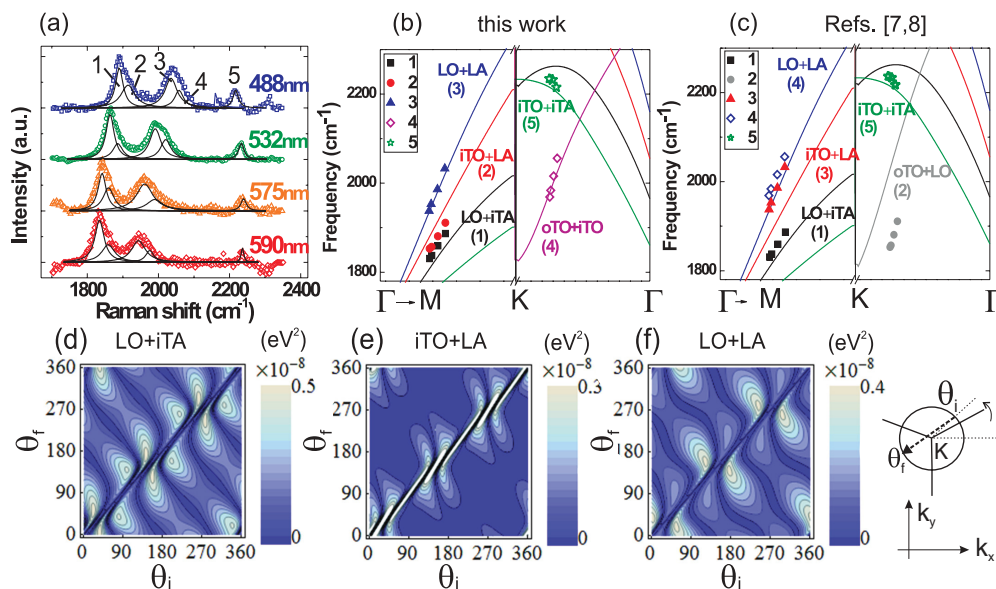


FIG. 1. (Color online) (a) The Raman spectra for the combination modes in the frequency region from 1700 to 2300 cm^{-1} for four different laser lines: 488 nm (2.54 eV), 532 nm (2.33 eV), 575 nm (2.16 eV), and 590 nm (2.10 eV). In (b) and (c) we show the predicted phonon dispersion of single-layer graphene (SLG) (solid lines) adapted from Popov and Lambin,²⁷ showing the phonon branches near the Γ point (left) and near the \mathbf{K} point (right) for the combinations modes LO + iTA (black), iTO + LA (red), LO + LA (blue), oTO + iTO (purple), oTO + LO (gray), and iTO + iTA (green). (b) The phonon assignments of the present work for the experimental results obtained from the spectra in (a). Squares correspond to peak 1, circles to peak 2, triangles to peak 3, and diamonds and stars to peaks 4 and 5, respectively. Peaks 1, 2, and 3 come from an intravalley (AV) DRR process, while peaks 4 and 5 come from an intervalley (EV) DRR process. (c) The experimental data from this work are plotted considering the assignments proposed in the literature^{7,8}: Peaks 1, 3, and 4 coming from an intravalley DRR process and peaks 2 and 5 coming from an intervalley DRR process, which is different from the assignment in (b). The peak numbers are written below the corresponding phonon branch assigned to that peak. The absolute values for the angular dependence of the intravalley el-ph scattering matrix elements for the (d) LO + iTA (peak 1), (e) iTO + LA (peak 2), and (f) LO + LA (peak 3) phonon combination modes for $E_L = 2.54$ eV. θ_i and θ_f are, respectively, the initial and final scattering angles measured at the \mathbf{K} point relative to the k_x axis.

Here we propose different assignments for peaks 2, 3, and 4, and these new assignments are based on and supported by phonon self-energy renormalization phenomena and by angle-dependent el-ph scattering matrix element calculations that provide more precise information that was not considered in the previous works.^{7,8} It is worth commenting that these angle-dependent scattering calculations give us the region (which can be associated with a high-symmetry direction) along which the scattering processes have the highest probability of happening [see the brightest spots in the calculated Figs.

1(d)–1(f) and the calculated Figs. 2(d)–2(f), where θ_i and θ_f are, respectively, the initial and final scattering angles at the \mathbf{K} point measured from the k_x axis]. Note that to determine those scattering regions the angle-dependent calculation was done considering all the possible directions in the two-dimensional BZ. Here we chose, for providing intuitive guidance, the direction along the $\Gamma\mathbf{K}\mathbf{M}$ line that describes better the region of the main scattering contribution given by the el-ph matrix elements. Using this strategy we can satisfactorily extract from the matrix elements calculations whether the main

TABLE I. Combination mode assignments, including a region in the BZ, scattering directions, and dispersion (units given in cm^{-1}/eV) for the five $q \neq 0$ combination Raman modes in single-layer graphene (SLG) from this work and from works published in the literature.^{7,8}

Peaks ($\omega_q \text{ cm}^{-1}$) ^a	1 (1887)	2 (1913)	3 (2036)	4 (2064)	5 (2214)
This work	LO + iTA	iTO + LA	LO + LA	oTO + iTO	iTO + iTA
BZ point	Γ	Γ	Γ	\mathbf{K} ($\mathbf{K}\Gamma$)	\mathbf{K} ($\mathbf{K}\mathbf{M}$)
Dispersion	128 ± 2	135 ± 6	213 ± 5	214 ± 5	-50 ± 5
Cong <i>et al.</i> ⁷	LO + iTA	–	iTO + LA	LO + LA	–
BZ point	Γ	–	Γ	Γ	–
Dispersion	140	–	198	221	–
Rao <i>et al.</i> ⁸	LO + iTA	oTO + LO	iTO + LA	LO + LA	iTO + iTA
BZ point	Γ	\mathbf{K}	Γ	Γ	\mathbf{K}
Dispersion	135	150	204	223	–56

^aAll the peak position references for this table were taken with the laser line 488 nm (2.54 eV).

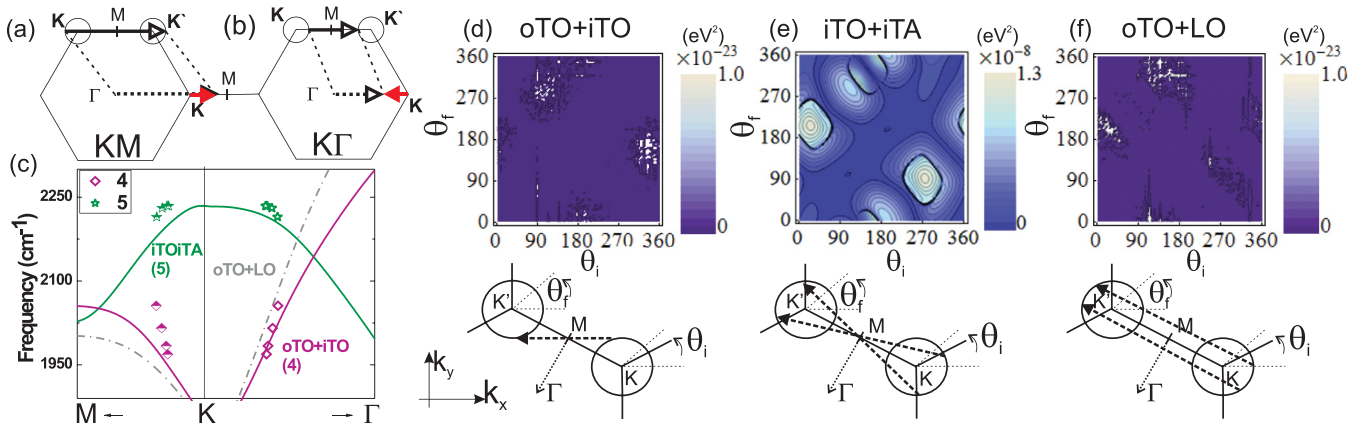


FIG. 2. (Color online) DRR processes involving phonons in the (a) **KM** or in the (b) **K Γ** direction, respectively, measured from the **K** point (red full arrows). (c) The phonon dispersion relation for the two intervalley (EV) combination modes: Peaks 4 (purple diamonds) and 5 (green stars). The half-colored symbols correspond to the DRR process in the **KM** direction and the open symbols correspond to the DRR process in the **K Γ** direction. The absolute value for the angular dependence of the EV el-ph scattering matrix elements for the (d) oTO + iTO, (e) iTO + iTA, and (f) oTO + LO phonon combination modes for $E_L = 2.54$ eV. θ_i and θ_f are, respectively, the initial and final scattering angles relative to the k_x axis. The diagrams below (d), (e), and (f) show the scattering regions for which the el-ph matrix elements for the particular combination mode are maximum.

phonon scattering process is closer to the **KM** or to the **K Γ** direction, and this can prevent us from making any mistakes in the phonon combination mode assignments as well as from eliminating some combination modes from the possible list of choices for the possible assignments (Appendix B provides a detailed description of how the angle-dependent el-ph matrix elements are calculated). From Fig. 1(b) we can see that the experimental peak 2 (red circles) is in better agreement with the combination phonon branch iTO + LA around the Γ point. Also, as shown in Fig. 1(b), by comparing the experimental and the theoretical phonon dispersions, we can see that peak 3 matches more accurately the phonon branch LO + LA around the Γ point, while peak 4 is in good agreement with the intervalley DRR process around the **K** point involving the oTO + iTO phonons. In Table I we summarize the new assignments found in this work and compare these to the assignments published in the literature for SLG.^{7,8} Also given in Table I are values for the E_L -dependent phonon dispersion rate ($\partial\omega/\partial E_L$) for each combination mode. The most likely el-ph scattering directions are also addressed for the intervalley DRR processes assigned in this work and included in the table as **K Γ** and **KM**.

Note that, in order to give reliability to some combination mode assignments, as is the case for peaks 4 and 5, it is also important to specify the direction along which the scattering process is most likely happening. As discussed above, we have assigned peaks 4 and 5, respectively, as the oTO + iTO and iTO + iTA $q \neq 0$ combination modes around the **K** point generated by an intervalley (EV) process. The phonon wave vector which is mainly involved in the DRR process lies very close to either the **KM** or the **K Γ** directions (this is why we are considering the high-symmetry directions, for simplicity) measured from the **K** point^{29,30} [see Figs. 2(a) and 2(b) for the distinction between a **K Γ** and a **KM** process]. In Fig. 2(c) we plot the experimental phonon dispersion for peaks 4 and 5 considering both the **KM** and **K Γ** directions.

Besides the different assignments among the various peaks, our results differ from the results in the literature^{7,8} specially because we use the oTO + iTO combination mode instead of the oTO + LO combination mode proposed in Ref. 8.

Figure 2(c) shows that for peak 4 the agreement between the experimental data and the theoretical phonon dispersion strongly suggests that the scattering events are happening in the **K Γ** direction. However, it could be hard to decide whether it is the oTO + LO or the oTO + iTO combination that gives the correct assignment for this phonon mode since the frequencies of these combination modes and their dispersions are very close to each other. In our assignment we use the fact that the directions of the el-ph matrix elements with the largest values, as well as their phonon self-energy corrections studied by varying E_F (as shown later in the text), are different for oTO + LO and oTO + iTO. Figures 2(d), 2(e), and 2(f) show the absolute values for the angular dependence of the EV el-ph matrix elements for the oTO + iTO, iTO + iTA, and oTO + LO phonon combination modes for $E_L = 2.54$ eV, where θ_i and θ_f are, respectively, the initial and final scattering angles defined at the **K** and **K'** points [see Figs. 2(d)–2(f)]. The diagrams in Figs. 2(d)–2(f) show the scattering directions for which the el-ph matrix elements are maximum (brightest spots in the figures) for the corresponding combination mode. Looking at the el-ph matrix elements for the oTO + iTO combination mode in Fig. 2(d), we can see that the region for which the el-ph matrix elements are maximum is closer to the **K Γ** direction. On the other hand, if we look at the scattering diagram for the oTO + LO combination mode in Fig. 2(f), the el-ph matrix elements are a maximum closer to the **KM** direction. From Fig. 2(c) we can see a better agreement of peak 4 along **K Γ** than along the **KM** direction. Then, by first combining the el-ph matrix elements with the theoretical phonon dispersion, we can conclude that peak 4 comes from a DRR process involving the oTO + iTO phonon combination

mode in the $\mathbf{K}\Gamma$ direction. It is worth commenting that the matrix elements for the $\text{oTO} + \text{iTO}$ and $\text{oTO} + \text{LO}$ combination modes are much weaker than those for the $\text{iTO} + \text{iTA}$ modes because the oTO mode does not have strong el-ph coupling in graphene. However, we believe that the coupling of the oTO mode becomes stronger when the monolayer graphene is sitting on a substrate, so that the oTO mode couples to the substrate.³¹

In Fig. 2(c) the experimental data for peak 5 is seen to be close to the theoretical curve for both the $\mathbf{K}\Gamma$ and $\mathbf{K}M$ directions and we must use other information to decide the direction for which the main contribution to the Raman scattering occurs. In this case, the correct assignment is also decided based on the phonon renormalizations, the theoretical predictions for the scattering processes, and the most important el-ph matrix elements. In Fig. 2(e) we can see that the direction for the $\text{iTO} + \text{iTA}$ combination mode has a maximum close to the $\mathbf{K}M$ direction, from which we conclude that the main contribution to peak 5 comes from an intervalley DRR process in the $\mathbf{K}M$ direction.

B. Phonon self-energy analysis

Next we explore the phonon self-energies and the el-ph coupling for those combination modes, which turns out to be fundamental for verifying the accuracy of the assignment procedure. Figures 3(b), 3(e), and 3(f), respectively, show the experimental data for the dependence of the phonon frequency ω_q (black solid triangles) and the phonon decay width γ_q (open dots) on V_g (or on the Fermi energy) for the five combination

modes. The phonon frequencies of the combination modes are shown using the same scale so that a better comparison can be made regarding the strength of the phonon renormalization phenomena for each combination mode. The dashed lines are guides for the eyes. Figure 3(a) shows the gate-modulated response of the G band, consistent with previous works.^{16,17} The G band was monitored in order to estimate the charge neutrality or Dirac point position for each sample studied in this work. From Fig. 3(a) one can see that the minimum of the frequency occurs around 0 V, indicating the charge neutrality point. For the G band of monolayer graphene, when the charge carrier density increases, ω_G undergoes a hardening, while the γ_G narrows. This is explained on the basis of the phonon self-energy renormalization for zone center ($q = 0$, Γ point) phonons, in which an electron-hole (el-h) pair can be virtually created (annihilated) by a phonon absorption (emission) process.^{12,13,15–18} Because of the Pauli exclusion principle, when the charge concentration decreases (increases), the initial (final) state of the virtual creation of an el-h pair—whose energy now is smaller (larger) than the phonon energy—becomes unoccupied (occupied) and thus a hardening in the frequency ω_q and a narrowing of the decay width γ_q can be observed.¹⁶

In contrast, by observing Figs. 3(b) to 3(f), it is seen that ω_q is softened for all five Raman combination features from 1700 to 2300 cm^{-1} , and that the ω_q softening is accompanied by a broadening of γ_q with increasing carrier concentration (increasing $|V_g|$). Now, instead of the Pauli exclusion principle, the electronic and vibrational density of states (together with energy and momentum conservation requirements) are

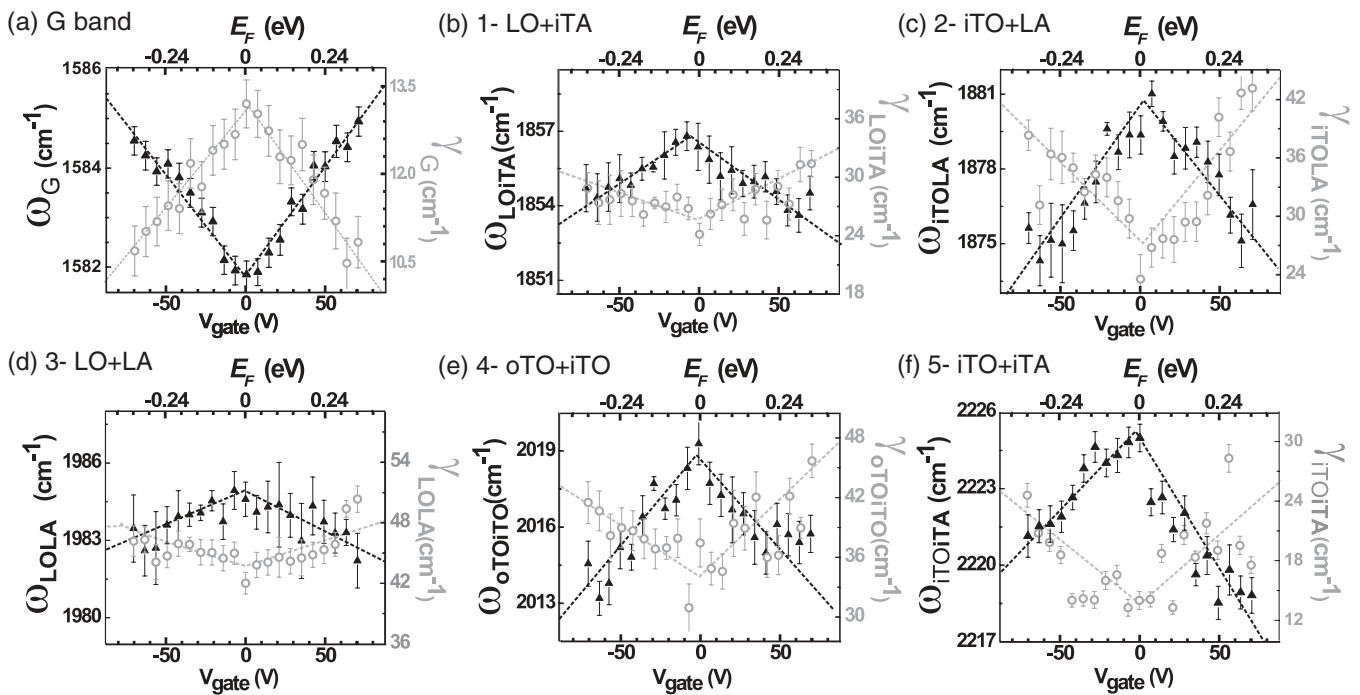


FIG. 3. The dependence of the phonon frequency ω_q (black solid triangles) and phonon decay width γ_q (open dots) on gate voltage (V_g) for the (a) G band and phonon combination modes (b) 1, (c) 2, (d) 3, (e) 4, and (f) 5. All the graphics, except for the G band, are on the same scale for better comparison between the phonon renormalization results for the five combination modes assigned in this work. Notice that all five combination modes [(b) through (f)] show a decrease of ω_q and a broadening of γ_q with increasing V_g . The dashed lines are guides for the eyes and the error bars come from the fitting procedure.

determining if the el-h pair creation (annihilation) due to a $q \neq 0$ phonon absorption (emission) will happen or not. In a previous work for ω_{G^*} , the 2450 cm^{-1} Raman feature,¹⁹ the authors explained that the behavior observed in the present work for all five combination modes is common to Raman modes that come from an AV or EV DRR process with $q \neq 0$ and is opposite to the behavior observed for the Γ point $q = 0$ phonons, such as for ω_G . Namely, for the $q \neq 0$ cases, when the Fermi level is around zero, either no el-h pair can be created by the absorption of a phonon (for an intravalley DRR process) or the probability of an el-h pair creation is very small (for an intervalley DRR process) because the density of states vanishes at the Dirac point. However, when the charge concentration increases, the renormalization of the phonon energy occurs by the creation of an el-h pair through the absorption of a phonon [Figs. 3(b) through 3(f)], then a softening of ω_q and a broadening of γ_q are observed, in contrast to what happens for $q = 0$ phonons at the Γ point.¹⁹

The results in Figs. 3(b)–3(f) confirm that the Raman combination modes come from a DRR process with $q \neq 0$ phonons, in accordance with the predictions of Ref. 19 and explanations given above. We also can see that the ω_q and γ_q renormalizations due to the change in the Fermi level position are weak for peak 1 [Fig. 3(b)] and peak 3 [Fig. 3(d)], when compared to the other three peaks. In accordance with the assignments given to the peaks and since both of these peaks involve the LO phonon branch, we can conclude that the coupling of this phonon to all the other relevant phonon modes is not large compared to the other peaks. Moreover, the LO mode is not expected to show a strong el-ph coupling when \mathbf{q} moves away from the Γ point (LO will present a strong coupling for $q = 0$ at the Γ point),¹⁴ which confirms the reason for our assignments to peaks 1 (LO + iTA) and 3 (LO + LA). It is worth saying that the acoustic modes have zero (small) energy at the Γ point (around Γ point) so that no (a negligible) contribution to the phonon renormalizations due to el-h pair creation could be expected coming from these acoustic modes.

On the other hand, the ω_q and γ_q renormalizations for peaks 2, 4, and 5 are of the same order of magnitude as that for the G band, which has a strong el-ph coupling.^{12,13,15–17} The behavior observed for peaks 4 (oTO + iTO) and 5 (iTO + iTA) is due to the strong el-ph coupling of the iTO phonon branch expected for the \mathbf{K} -point phonons in SLG. Another interesting observation: Peak 2 (iTO + LA), which is a $q \neq 0$ mode around the Γ point, shows that the renormalizations due to the iTO mode become strong when moving away from the Γ point. This is fully consistent with what we observed for peaks 1 and 3 around the Γ point. While the LO mode renormalization weakens, the iTO mode renormalization is strengthened in moving away from the Γ point (remember that for $q = 0$ Γ -point phonons, LO has a strong renormalization while the iTO has not). The observed gate-dependent behavior consistently confirms the assignments given to the combination modes in this work since there is a consistency between the phonon modes assigned to each peak and the strength of the el-ph coupling in each mode. This result shows that the gate-modulated Raman scattering is indeed a powerful technique to confirm the phonon mode assignments attributed to Raman peaks when the gate voltage and E_L dependence are both

measured. This is clearly the case for peaks 3 and 4 in this work. It is worth mentioning that, especially as regards peak 4, the gate-modulated results are important to decide which is the correct combination mode assignment for peak 4. This feature could have been assigned to the oTO + LO phonon combination mode, as stated earlier.⁸ However, if the oTO + LO assignment were correct, the el-ph coupling would be expected to be similar to what is seen in Figs. 3(b) and 3(d), which are combinations that contain the LO phonon mode. Note that the oTO mode is not expected to show a strong el-ph coupling around the \mathbf{K} point.¹⁴ The sizable renormalization effect seen experimentally in Fig. 3(e) therefore strengthens the oTO + iTO choice for the combination mode assignment of peak 4.

IV. SUMMARY

In summary, we have done Raman measurements with different gate voltages V_g and different laser excitation energies E_L in single-layer graphene and we have shown that there are five observable combination Raman modes in the region from 1700 to 2300 cm^{-1} . By exploring the $q \neq 0$ phonon anomalous self-energy corrections and by comparing the experimental data with the theoretical phonon dispersion and making use of the angle-dependent electron-phonon (el-ph) scattering calculations, we have assigned the first three peaks [see Fig. 1(a)], respectively, to the intravalley combination modes LO + iTA, iTO + LA, and LO + LA around the Γ point of the Brillouin zone and peaks 4 and 5 to the intervalley oTO + iTO and iTO + iTA combination modes around the \mathbf{K} point of the Brillouin zone, respectively. Namely, the main contribution of the DRR process for peak 4 (assigned as oTO + iTO in this work) is in the $\mathbf{K}\Gamma$ direction, while peak 5 (assigned as iTO + iTA in this work) is attributed to the predominant Raman intensity coming from the \mathbf{KM} direction. For all five phonon combination modes, we observed an anomalous phonon self-energy renormalization, where a decrease of the phonon frequency and a broadening of the phonon decay width with increasing gate voltage occurs, as is predicted for a double resonance Raman process with $q \neq 0$ wave vectors.¹⁹ We show that the el-ph coupling is larger for peaks 2, 4, and 5 mostly due to the strong el-ph coupling of the iTO phonon branch. The phonon frequency and decay width renormalizations for peaks 1 and 3 are small due to the weak el-ph coupling of the LO phonon branch. These el-ph dependencies on gate voltage support our assignments when compared to the assignments in the current literature.^{7,8} We believe that this work resolves the discussion of assignments for these combination modes in single-layer graphene, thereby resolving a recent discussion in the literature.^{7,8} Moreover, these results launch gate-modulated Raman as an approach to identify and assign phonon modes in solid state materials. This technique will certainly contribute to the understanding of more complex structures such as few-layer graphene, their stacking order relations, as well as how these stacking orders influence the many-body interactions in the system. Moreover, the techniques reported here can become a key strategy to study and understand a whole class of new layered 2D materials, such as molybdenum sulfide (MoS_2), hydroxides, and oxides in general, now emerging in the scientific community.³²

ACKNOWLEDGMENTS

D.L.M. acknowledges the support from CNPq-Brazil, SM Projetos LTDA and NSF - DMR 10-04147. P.T.A. acknowledges the support from CNPq-Brazil and ONR MURI N00014-09-1-1063, R.S. and K.S. acknowledge MEXT Grants No. 20241023 and No. 23710118, respectively. M.S.D. acknowledges MURI N00014-09-1-1063.

APPENDIX A: DETERMINATION OF THE PHONON WAVE VECTOR q

To determine the phonon wave vector q from the E_L -dependent experiment, we need to consider the electronic dispersion of monolayer graphene around the \mathbf{K} point given, as a first approximation, by^{4,22,23}

$$E(\mathbf{k}) = \hbar v_F \left\{ \frac{(1.2)}{3a} \pm |\mathbf{k}| - \left[\frac{(0.6)a}{2} \pm \frac{a}{4} \sin(3\theta_k) \right] |\mathbf{k}|^2 \right\}, \quad (\text{A1})$$

where $a = 1.42 \text{ \AA}$ is the carbon-carbon distance and θ_k is defined as shown in Fig. 4(c) and its value is obtained from the angle-dependent el-ph matrix elements calculations. As shown in Fig. 4, the combination mode assignment is performed by considering the equations for the energy and momentum conservation of the double resonance process conditions^{22,23}

$$E_L = \hbar\omega_L = 2\hbar v_F \left[|\mathbf{k}| - \frac{a}{4} \sin(3\theta_k) |\mathbf{k}|^2 \right], \quad (\text{A2})$$

where $k = k_0$ for a vertical transition, where an electron goes from the valence to the conduction band by absorbing a photon with energy E_L :

$$\hbar\omega_{\text{ph}} = \hbar v_F \left[|\mathbf{k} - \mathbf{k}'| - \frac{a}{4} \sin(3\theta_k) (|\mathbf{k}|^2 - |\mathbf{k}'|^2) \right]. \quad (\text{A3})$$

Here a phonon scatters the electron from the electronic state \mathbf{k} to \mathbf{k}' , and the wave vector

$$\mathbf{q} = \mathbf{k} + \mathbf{k}', \quad (\text{A4})$$

which can be measured from either the Γ or the \mathbf{K} point depending on whether the scattering process is an intravalley or intervalley process, respectively (see Fig. 4). Here \mathbf{k} and \mathbf{k}' are the wave vectors of the initial and the final electronic state

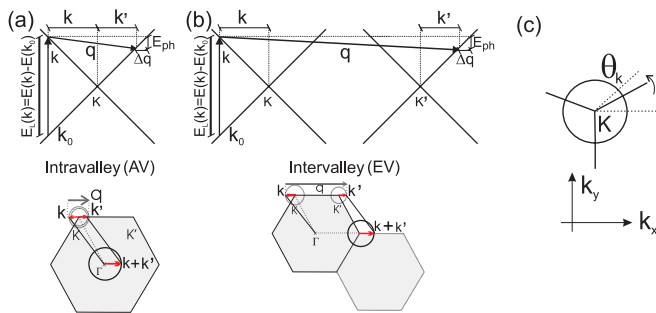


FIG. 4. (Color online) Determination of the phonon wave vector q for (a) intravalley (AV) and (b) intervalley (EV) double resonance Raman processes. Namely, k_0 , k , and k' stand for the electronic wave vectors and $E(k)$ is the electronic dispersion given by Eq. (A1). (c) θ_k is defined with relation to the k_x axis.

involved in the scattering process, respectively. By combining the three equations (A2), (A3), and (A4) above, we can relate directly the laser frequency $\omega_L = E_L/\hbar$ with the phonon wave vectors q , measured from the Γ point in the case of an AV process or from the \mathbf{K} point in the case of an EV process.³³ Note that the ω_L and ω_{ph} values are obtained from the experiment.

APPENDIX B: THEORETICAL DETAILS FOR THE CALCULATION OF THE ANGLE-DEPENDENT ELECTRON-PHONON MATRIX ELEMENTS

It is important to understand the angular dependence of the el-ph matrix elements because they generally depend on both the k (electron) and q (phonon) wave vectors. The calculation method for determining the el-ph matrix elements and how to obtain the q vector is well established in previous works.^{33,34} It is worth commenting that the purpose of the calculation in this paper is to specify the region in k space in which the phonon wave vector q most strongly contributes to the double resonance Raman scattering, so that we can properly assign the combination modes. In the calculations we consider not only the $\Gamma\mathbf{K}\mathbf{M}$ line to obtain the q directions but the entire Brillouin zone is included in the actual calculations. However, it is important to note that theory tells us that because of the hexagonal symmetry in k space, the maximum el-ph values are always found near the high-symmetry lines. For this reason we include a physical discussion in this paper to provide a better understanding of the interpretation of the Raman spectra.

For a more physical understanding of the underlying theory used in this work, let us recall how the optical process of double resonance Raman spectra happens: For a given laser energy, (1) a circle that represents an electronic equienergy contour (or a circle that is deformed by the trigonal warping effect) around the \mathbf{K} or \mathbf{K}' points is selected for possible k vectors that might be especially important for the experiment (see Fig. 5); (2) then another equienergy circle (or deformed circle) with an energy separation ($E_L - E_{\text{ph}}$) around the \mathbf{K} or \mathbf{K}' points is selected for possible k' vectors; (3) the phonon wave vector q must satisfy the momentum conservation requirement $q = k - k'$; and (4) the el-ph matrix element for the Raman intensity is calculated for $M_{\text{el-ph}}(k, k - q)$ or $M_{\text{el-ph}}(k - q, k)$, which are both q and k dependent. Based on these assumptions, we use first-order perturbation theory to calculate the el-ph matrix element by assuming that this matrix element is given by the potential variation due to the lattice vibration.³⁴ The double resonance Raman intensity for combination and phonon mode overtone

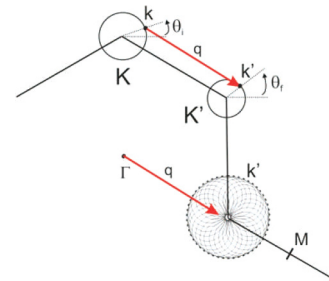


FIG. 5. (Color online) All the possible final electronic states k' for a given initial electronic state k .

relies on the el-ph interaction as follows:⁵

$$I(\omega_1, \omega_2, E_L) = \sum_j \left| \sum_{|a,b,\omega_1,\omega_2} \frac{M_{\text{el-op}}(j,c)M_{\text{el-ph}}(c,b)M_{\text{el-ph}}(b,a)M_{\text{el-op}}(a,j)}{\Delta E_{aj}(\Delta E_{bj} - \hbar\omega_1)(\Delta E_{aj} - \hbar\omega_1 - \hbar\omega_2)} \right|^2, \quad (\text{B1})$$

where $\Delta E_{aj} = E_L - (E_a - E_j) - i\gamma$ and E_L is given by Eq. (A2).

Here the indices j , a , b , and c denote, respectively, the initial, the excited, and the first and second scattered electronic states. Also, γ is the broadening factor, ω_1 and ω_2 are the phonon frequencies (if $\omega_1 \neq \omega_2$, a combination of phonon modes is considered; if $\omega_1 = \omega_2$, we have an overtone), and $M_{\text{el-op}}$ and $M_{\text{el-ph}}$ in Eq. (B1) are the electron-photon and electron-phonon matrix elements, respectively. It is worth mentioning that in order to calculate the relative Raman intensity given by Eq. (B1) we need to integrate over the entire Brillouin zone and over all the possible electronic states, which is very time consuming and it is not necessary to evaluate the dominant scattering directions. It must be understood that once we have defined the equienergies around \mathbf{K} or \mathbf{K}' , we must consider all the possible directions for a phonon with momentum q to connect k and k' , such that $q = k - k'$ with k and k' coming from the determined equienergies. As shown in Fig. 5 for each θ_i (which indexes the initial electronic state k) we need to consider all θ_f (which indexes the final electronic

state k') to properly evaluate $M_{\text{el-ph}}$, which is dependent of both θ_i and θ_f .

Since we have previously set the electronic equienergies so that the electronic resonance occurs, we restricted our detailed calculations to the equienergy circles around \mathbf{K} or \mathbf{K}' which give zero energy denominators in Eq. (B1). Any substantial change in Eq. (B1) to the calculated scattering intensity will be related to $M_{\text{el-ph}}$. Therefore, the larger the $M_{\text{el-ph}}$ (which depends on both θ_i and θ_f), the larger the output of Eq. (B1). The electron-phonon matrix elements $M_{\text{el-ph}}$ are given over all the possible directions in the two-dimensional Brillouin zone (BZ). Therefore, even though we are considering only the high-symmetry line in detail, we can satisfactorily extract from the matrix elements calculations information about whether the main phonon scattering process is closer to the \mathbf{KM} or $\mathbf{K}\Gamma$ directions, and this information can prevent us from making any mistakes in both the combination mode and overtone phonon mode assignments as well as in the possible elimination of some combination modes from the possible list of choices for possible assignments of these Raman features.

*Corresponding author: ptaraujo@mit.edu

¹F. Tuinstra and J. L. Koenig, *J. Phys. Chem.* **53**, 1126 (1970).

²R. J. Nemanich and S. A. Solin, *Phys. Rev. B* **20**, 392 (1979).

³M. S. Dresselhaus, G. Dresselhaus, K. Sugihara, I. L. Spain, and H. A. Goldberg, *Graphite Fibers and Filaments*, Springer Series in Materials Science, Vol. 5 (Springer, Berlin, 1988).

⁴R. Saito, G. Dresselhaus, and M. S. Dresselhaus, *Physical Properties of Carbon Nanotubes* (Imperial College Press, London, 1998).

⁵M. S. Dresselhaus, G. Dresselhaus, R. Saito, and A. Jorio, *Phys. Rep.* **409**, 47 (2005).

⁶A. C. Ferrari, J. C. Meyer, V. Scardaci, C. Casiraghi, M. Lazzeri, F. Mauri, S. Piscanec, D. Jiang, K. S. Novoselov, S. Roth, and A. K. Geim, *Phys. Rev. Lett.* **97**, 187401 (2006).

⁷C. Cong, T. Yu, R. Saito, G. Dresselhaus, and M. S. Dresselhaus, *ACS Nano* **5**, 1600 (2011).

⁸R. Rao, R. Podila, R. Tsuchikawa, J. Katoch, D. Tishler, A. M. Rao, and M. Ishigami, *ACS Nano* **5**, 1594 (2011).

⁹K. Sato, J. S. Park, R. Saito, C. Cong, T. Yu, C. H. Lui, T. F. Heinz, G. Dresselhaus, and M. S. Dresselhaus, *Phys. Rev. B* **84**, 035419 (2011).

¹⁰C. H. Lui, L. M. Malard, S. H. Kim, G. Lantz, F. E. Laverge, R. Saito, and T. F. Heinz, *Nano Lett.* **12**, 5539 (2012).

¹¹C. Cong, T. Yu, K. Sato, J. Shang, R. Saito, G. Dresselhaus, and M. S. Dresselhaus, *ACS Nano* **5**, 8760 (2011).

¹²T. Ando, *J. Phys. Soc. Jpn.* **75**, 024707 (2006).

¹³M. Lazzeri and F. Mauri, *Phys. Rev. Lett.* **97**, 266407 (2006).

¹⁴S. Piscanec, M. Lazzeri, F. Mauri, A. C. Ferrari, and J. Robertson, *Phys. Rev. Lett.* **93**, 185503 (2004).

¹⁵S. Pisana, M. Lazzeri, C. Casiraghi, K. S. Novoselov, A. K. Geim, A. C. Ferrari, and F. Mauri, *Nat. Mater.* **6**, 198 (2007).

¹⁶J. Yan, Y. Zhang, P. Kim, and A. Pinczuk, *Phys. Rev. Lett.* **98**, 166802 (2007).

¹⁷A. Das, S. Pisana, B. Chakraborty, S. Piscanec, S. K. Saha, U. V. Waghmare, K. S. Novoselov, H. R. Krishnamurthy, A. K. Geim, A. C. Ferrari, and A. K. Sood, *Nat. Nanotech.* **3**, 210 (2008).

¹⁸K. I. Sasaki, M. Yamamoto, S. Murakami, R. Saito, M. S. Dresselhaus, K. Takai, T. Mori, T. Enoki, and K. Wakabayashi, *Phys. Rev. B* **80**, 155450 (2009).

¹⁹P. T. Araujo, D. L. Mafra, K. Sato, R. Saito, J. Kong, and M. S. Dresselhaus, *Phys. Rev. Lett.* **109**, 046801 (2012).

²⁰L. M. Malard, M. A. Pimenta, G. Dresselhaus, and M. S. Dresselhaus, *Phys. Rep.* **473**, 51 (2009).

²¹A. V. Baranov, A. N. Bekhterev, Y. S. Bobovich, and V. I. Petrov, *Opt. Spektrosk.* **62**, 1036 (1987).

²²C. Thomsen and S. Reich, *Phys. Rev. Lett.* **85**, 5214 (2000).

²³R. Saito, A. Jorio, A. G. Souza Filho, G. Dresselhaus, M. S. Dresselhaus, and M. A. Pimenta, *Phys. Rev. Lett.* **88**, 027401 (2001).

²⁴R. Saito, A. Grüneis, G. G. Samsonidze, V. W. Brar, G. Dresselhaus, M. S. Dresselhaus, A. Jorio, L. G. Cançado, C. Fantini, M. A. Pimenta, and A. G. Souza Filho, *New J. Phys.* **5**, 157 (2003).

²⁵M. A. Pimenta, G. Dresselhaus, M. S. Dresselhaus, L. G. Cançado, A. Jorio, and R. Saito, *Phys. Chem. Chem. Phys.* **9**, 1276 (2007).

- ²⁶R. Saito, M. Hofmann, G. Dresselhaus, A. Jorio, and M. S. Dresselhaus, *Adv. Phys.* **60**, 413 (2011).
- ²⁷V. N. Popov and P. Lambin, *Phys. Rev. B* **73**, 085407 (2006).
- ²⁸K. S. Novoselov, A. K. Geim, S. V. Morozov, D. Jiang, Y. Zhang, S. V. Dubonos, I. V. Grigorieva, and A. A. Firsov, *Science* **306**, 666 (2004).
- ²⁹J. Maultzsch, S. Reich, and C. Thomsen, *Phys. Rev. B* **70**, 155403 (2004).
- ³⁰D. L. Mafra, E. A. Moujaes, S. K. Doorn, H. Htoon, R. W. Nunes, and M. A. Pimenta, *Carbon* **49**, 1511 (2011).
- ³¹The authors are now calculating the influence of the substrate on the observed Raman combination modes that includes the oTO mode.
- ³²R. Ma and T. Sasaki, *Adv. Mater.* **22**, 5082 (2010).
- ³³D. L. Mafra, G. Samsonidze, L. M. Malard, D. C. Elias, J. C. Brant, F. Plentz, E. S. Alves, and M. A. Pimenta, *Phys. Rev. B* **76**, 233407 (2007).
- ³⁴J. Jiang, R. Saito, G. G. Samsonidze, S. G. Chou, A. Jorio, G. Dresselhaus, and M. S. Dresselhaus, *Phys. Rev. B* **72**, 235408 (2005).